Preprint, Astrophysical Journal, in press July 2002

Density and Velocity Structure of the Be Star Equatorial Disk in the Binary, LS I +61°303, a Probable Microquasar

P. C. Gregory and C. Neish

Department of Physics and Astronomy, University of British Columbia, Vancouver, British Columbia, V6T 1Z1, Canada

gregory@physics.ubc.ca
cdneish@interchange.ubc.ca

ABSTRACT

We explore a new method for investigating the density and velocity structure of the Be star equatorial disk in LS I +61°303, based on its variable radio emission. At a particular radius the method yields a circularly shaped solution locus in the radial (v_r) and circular (v_c) components of the disk gas velocity, which allows us to set limits on v_r and v_c at that radius. For a given model of the circular velocity, $v_c(r)$, we can derive $v_r(r)$ and the gas density, $\rho(r)$ within a constant. While $\rho(r)$ depends on the assumed model for $v_c(r)$, we find the fractional change in gas density at any radius does not. This allows us to study the evolution in $\rho(r)$ with time. The analysis indicates that the previously demonstrated ~ 4.6 year modulation in radio properties results from an outward moving density enhancement or shell in the equatorial disk with a velocity of ~ 1.0 km s^{-1}. We propose that each new shell ejection may be triggered by the interaction of a short lived relativistic wind (ejector phase) from the neutron star, with the rapidly rotating Be star. Our best estimates of the mass accretion rate of the neutron star are in the range ~ 0.001 to ~ 0.01 of the Eddington accretion limit. This translates to an expected luminosity range of $\sim 10^{35}$ to $\sim 10^{36}$ ergs s^{-1} which is comparable to estimates of the total X-ray and γ-ray luminosity for LS I +61°303.

Subject headings: stars:emission-line — radio continuum:stars— Xrays:binaries— methods:data analysis

1. Introduction

In 1977, the highly variable radio source GT 0236+610 was discovered during a survey of the galactic plane for variable radio emission (Gregory and Taylor 1978). Based on an accurate radio position, GT 0236+610 was identified with LS I +61°303 (Gregory et al. 1979), an emission line star at a distance of 2.3 kpc (Frail and Hjellming 1991, Steele et al. 1998). Based on IUE ultraviolet and ground based spectroscopy, Hutchings and Crampton (1981) classified the primary as B0-B0.5 main sequence star with a high rotation velocity, undergoing mass loss through an equatorial disk. It exhibits unusually broad, double-peaked, and variable H_α and H_β emission lines. More recently, Howarth (1983) classified the star as a B4.5 III, while the photometric analysis of Paredes and Figueras (1986) is consistent with a B0-B0.5 III or B0 V primary star.

LS I +61°303 is one of a group of about 20 Be X-ray binary systems (van den Heuvel and Rappaport 1987). These systems have orbital periods of tens of days or longer, and the X-ray emission is considered to arise from wind accretion onto a neutron star companion. Approximately half of these objects show direct evidence for a neutron star companion in the form of X-ray pulsations. The non-pulsed emission is generally transient or highly variable with outburst durations similar to the orbital periods, luminosities in the keV range of $10^{36} - 10^{38}$ erg s^{-1} and hard spectra (kT $\sim 10 - 20$ keV). These outbursts are thought to occur as a result of increased wind accretion rates on the neutron star companion due to a combination of orbital eccentricity and irregular episodes of enhanced equatorial mass loss from the Be star (see van den Heuvel 1994).

LS I +61°303 distinguishes itself from other members of the group by its strong outbursting radio emission. The radio outbursts exhibit a period of 26.496 days (e.g., Taylor and Gregory 1982, Gregory 2002), which is interpreted as the orbital period. The phase and peak flux density of these outbursts are known to exhibit a ~ 4.6 year periodic modulation (e.g., Gregory et al. 1999, Gregory 2002). Zamanov and Martí (2000) have also recently demonstrated a modulation on the same time scale, in the EW(H_α) and $\Delta V_{\rm peak}$, the H$_\alpha$ equivalent width and double peak velocity separation, respectively. This latter results strongly suggests that the modulation in the radio emission is related to changes in the Be star equatorial disk properties.

The X-ray emission of LS I +61°303 (e.g. Taylor et al. 1996, Leahy et al. 1997, Harrison et al, 2000) is weak (10^{34} erg s^{-1} at maximum), compared to other members of the group. The 0.1-2.5 keV X-ray emission has been observed to vary by a factor of 10 over one orbital period (Taylor et al. 1996), but no X-ray pulsations have been detected. Paredes et al. (1997) reported an approximately 5 fold 26.7 ± 0.2 day modulation in the RXTE/ASM 2-10 keV X-ray flux. A more recent analysis of 1881 days of RXTE/ASM data (Leahy 2001)

yielded a period of 26.415 ± 0.05 days, which is consistent with the more accurate period derived from the radio data of 26.496 ± 0.0028 days (Gregory 2002). Within the measurement uncertainties the X-ray maximum always occurs at a constant orbital phase associated with periastron.

The ASCA observations of Leahy et al. (1997) show that the 0.5-10 keV spectrum is best described by a relatively hard power-law, and therefore the emission mechanism is non-thermal in nature. Their power-law spectral fit also yields a hydrogen column density of $\simeq 5 - 6 \times 10^{21}$ cm^{-2} which is in good agreement with the column density of 10^{22} cm^{-2} measured in the radio by Frail and Hjellming (1991). LS I +61°303 is also the probable counterpart to the γ-ray source, 2CG 135+01 (e.g., Gregory and Taylor 1978, Kniffen et al. 1997). If the COS-B γ-ray emission is associated with LS I +61°303 then γ- ray luminosities of $10^{36} - 10^{37}$ erg s^{-1} in the > 100 MeV range are inferred [1]. While these luminosities are similar to other high-mass X-ray binaries, the shift to higher photon energies points to some fundamental difference in the X-ray/γ-ray emission process.

A variety of models have been proposed to explain the observations. Maraschi and Treves (1981) discussed a model in which the companion is a moderately young pulsar and the relativistic electrons responsible for the radio emission are produced by the interaction of the relativistic wind of the neutron star and the normal wind from the primary. Lipunov and Nazin (1994) proposed a model in which relativistic electrons injected by a radio pulsar are captured by the magnetosphere of the Be star near periastron passage where they are cooled slowly by synchrotron losses. Paredes et al. (1991) employed a van den Laan adiabatic expansion model modified to include particle injection over an extended interval of the orbit.

Taylor and Gregory (1982, 1984) proposed a model in which the periodic radio outbursts result from variable accretion onto a compact companion in an eccentric orbit (e ~ 0.8) with a semi-major axis of about 5×10^{12} cm. Taylor et al. (1992) computed the accretion rate on to a neutron star secondary in orbit within the equatorial wind of the Be star primary for a variety of eccentricities. For $e > 0.4$ two accretion peaks occur. The biggest corresponds to periastron passage through the densest portion of the wind and a second smaller peak occurs at a later phase when the relative velocity of receding neutron star and the Be star wind is a minimum. Martí and Paredes (1995) investigated the variation of this structure with Be star equatorial wind velocity and found that both the height and delay of the second peak is a function of the Be star wind velocity. A variation of wind velocity from 20 to 2 km/s results in a variation in the radio phase of the peak from 0.62 to 0.92 for $e = 0.7$. Also the secondary

[1]Recently, Leahy et al. (1997) estimated the radio to 200 MeV γ-ray luminosity of LS I +61°303 at $\simeq 10^{35}$ erg s^{-1}.

peak is higher and narrower the larger the wind velocity [2]. Relativistic electrons produced near periastron will suffer severe inverse-Compton losses (e.g. Taylor et al. 1992, Martí and Paredes 1995, Leahy et al. 1997) from scattering off photons in the radiation field of the primary, giving rise to X-ray and $\gamma-$ray energies. Thus near periastron we expect an X-ray and possible gamma-ray outburst but very little in the way of radio emission. The available X-ray observations all exhibit a maximum around periastron. For the second accretion peak the neutron star is further from the primary and inverse-Compton losses will be much less.

LS I $+61°303$ also exhibits ~ 4.6 year periodic modulation of the phase and peak flux density of these radio outbursts (e.g. Gregory 1999, Gregory et al. 1999). The shape of the peak flux density modulation is sinusoidal in appearance while the phase modulation exhibits a saw-tooth waveform. Recently Gregory (2002, hereafter paper III) reported improved Bayesian estimates of both the orbital period P_1, and modulation period, P_2, based on the full Green Bank Interferometer (GBI) data set and improved estimates of the outburst times and peak flux densities. The new estimates are $P_1 = 26.4960 \pm .0028$ days and $P_2 = 1667 \pm 8$ days. That paper reached a number of conclusions which are important for the current paper, that are listed below.

1. The peak radio emission in each orbit occurs somewhere in a range of P_1 radio (orbital) phase extending from ~ 0.4 to 0.9. The zero of radio phase is by convention Julian Day 2,443,366.775, the date of the first radio detection of the star.

2. Periastron passage is estimated from both the radio and X-ray measurements to occur at radio phase of ~ 0.4 which means that radio outburst peaks are confined to one half of the orbit extending from periastron to apastron.

3. The characteristic outburst profiles shown by the cross correlation templates are very broad, indicative of measurable accretion over all of the orbit.

4. The optical depth at 8.3 GHz is always $<< 1$ while the optical depth at 2.2 GHz can reach values of ~ 2.7.

5. A test of the precessing Be star model of Lipunov and Nazin (1994) indicates that it is unlikely to be the correct mechanism to explain the 1667 day periodic modulation and that the neutron star orbit is coplanar with the Be star equatorial disk.

---

[2]It should be noted, that in the analysis of Taylor et al. (1992) and Martí and Paredes (1995), the circular component of the equatorial wind velocity was assumed to be zero.

Massi et al. (2001) have found evidence for a jet like structure in their recent EVN observations of the source and estimated the intrinsic velocity at 0.4 c. It is tempting to suppose that the 1667 day modulation in the outburst peak flux density results from variations in Doppler beaming arising from jet precession. However, such a mechanism does not account for the observed saw tooth shaped modulation of the outburst orbital phase with the same period (Gregory 2002).

In the next section we present details of a method for exploring the velocity and density distributions of the Be star equatorial disk. We then extract these quantities for all of the GBI data and examine their average radial dependence. We also examine the dependence of these disk parameters on P_2 modulation phase. Finally we discuss the implications of these results with respect to models for LS I $+61°303$ and Be stars in general.

2. Method

In this section we present details of a method for exploring the velocity and density distributions of the Be star equatorial disk. This information is derived from variations in the synchrotron radio emission associated with accretion by a companion neutron star in an eccentric orbit which is co-planar with the disk. The method is based on the following assumptions.

1. For the purposes of this exploratory study we assume the following properties of the binary system following Martí and Paredes (1995). The mass and radius of the Be star are $M_* = 10M_\odot, R_* = 10R_\odot$ and $M_n = 1.4M_\odot$ for the mass of the companion neutron star. We adopt an orbital period $P_1 = 26.496$ days, an eccentricity, $e = 0.82$ (Martí and Paredes 1995), and a radio phase of periastron, $\phi_p = 0.4$ (Gregory, 2002). It should be emphasized that apart from the period, the other orbital parameters are very uncertain. Estimates of the eccentricity range from $0.3 - 0.87$. We have adopted the best orbital solution reported by Martí and Paredes (1995), but have also explored a less eccentric orbit (see discussion).

2. The radio flux density at 8.3 GHz, S, is directly proportional to $\dot{\mathrm{M}}_n$, the rate at which mass is accreted by the neutron star from the Be star equatorial disk. We write this as

$$S(r,t) = K(r)\dot{\mathrm{M}}_n(r,t), \tag{1}$$

where $K(r)$ is the constant of proportionality at a particular radius of the neutron star from the Be star. In principle $K(r)$ may be a function of radius for a variety of

reasons to do with different accretion regimes, inverse-Compton cooling of the radio emitting relativistic gas by Be star photons, and variable geometry (discussed further below). Equation (1) assumes a linear relationship between S and $\dot{\mathrm{M}}_n$. This requires the optical depth of the 8.3 GHz emission be always $<< 1$, which was established in paper III.

In general $S(r,t)$ will depend on the past history of $K(r)\dot{\mathrm{M}}_n(r,t)$ over an interval of time, τ, and a corresponding range in orbital radius Δr. In this exploratory study we will assume Δr is small compared to our bin size in orbital radius so that equation (1) applies. One indication that $\tau < 1$ day comes from high time resolution observations at 10.5 GHz (Gregory et al. 1979). On three occasions we observed a large step like flux density increase on a time scales of ~ 1 hour.

3. We assume that the equatorial disk is circularly symmetric. In this paper we examine (a) the average properties of the disk and (b) their variations from the average within nine P_2 phase bins. In case (a) we only require circular symmetry when the average is taken over all P_2 phase. In case (b) we will be averaging over the orbits within each of 9 P_2 phase bin, which will require circular symmetry when averaging over approximately 7 orbits or $\sim$ 185 days. In this study we neglect the effect of possible variations of $K(r)$ with P_2 phase.

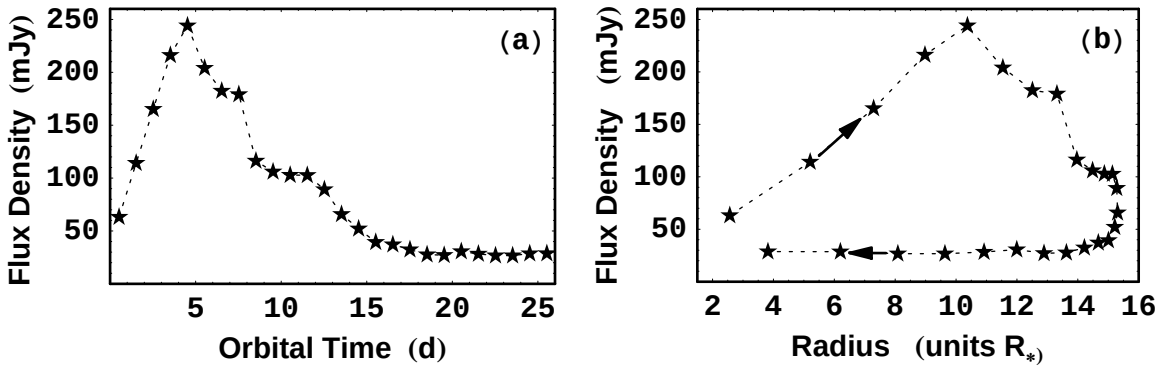

Fig. 1.— Panel (a) shows a typical outburst at 8.3 GHz as a function of time, which exhibits a rapid increase in flux density compared to the more gradual decline. Panel (b) shows the same outburst when viewed as a function of orbital radius. The arrows indicates the direction of increasing time.

What is our motivation for the second assumption? In the past we have employed the term outburst to characterize the variations in radio emission in each orbital cycle. The term lacks a precise definition but the chief characteristics of an outburst are perhaps best

represented by the giant radio outbursts from Cygnus X-3 (Gregory et al. 1972). These have been modelled by many authors as adiabatically expanding cloud of relativistic plasma with embedded magnetic field. On this basis an outburst is characterized by a rapid increase in flux density (optically thick phase) followed by a more gradual decay (optically thin phase), with the increase occurring at high frequencies first and the maximum progressively delayed at lower frequencies as a result of the increased opacity at lower frequencies. The term implies a short period of relativistic particle acceleration, although as mentioned in the introduction, Paredes et al. (1991) pointed out the need for continued particle injection over an extended interval in the case of LS I +61°303. In this paper we go a step further and argue that there is evidence for particle production throughout the entire orbit.

From 1994 January to 2000 October (Ray et al. 1997) detailed monitoring of LS I +61°303 was performed (several times a day)with the National Radio Astronomy Observatory Green Bank Interferometer (GBI) at 8.3 and 2.2 GHz. Panel (a) of Fig. 1 shows a typical outburst at 8.3 GHz as a function of time, which exhibits a rapid increase in flux density compared to the more gradual decline. For LS I +61°303 the optical depth at 8.3 GHz is always $<< 1$ so the increase in flux density is not consistent with the adiabatically expanding optically thick cloud model. Panel (b) shows the same outburst when viewed as a function of orbital radius. The arrows indicates the direction of increasing time. In these, perhaps more natural coordinates, the rise is if anything more gradual than the decay. The rapid rise when plotted as a function of time comes about as a result of the rapid motion of the neutron star near periastron in the very eccentric orbit. The radio emission is seen to vary continuously about the orbit, although it is much weaker on the inbound portion of the orbit.

The mass accretion rate, $\dot{\mathrm{M}}_n$, by a compact object traveling though a uniform density medium (Bondi and Hoyle, 1944) with density ρ is given by

$$\dot{\mathrm{M}}_n = \pi r_{acc}^2 v_{rel} \rho, \tag{2}$$

where the accretion radius, r_{acc}^2, is given by

$$r_{acc} = \frac{2GM_n}{v_{rel}^2}. \tag{3}$$

Here v_{rel} is the relative velocity of the neutron star, of mass M_n, to the gas in the equatorial disk. This equation assumes that r_{acc} is smaller than the length scale of the density and velocity variations. This is unlikely to be the case in the current problem for all orbital radii, but we will continue to use this relationship for $\dot{\mathrm{M}}_n$ and simply absorb any departures from this relationship in the $K(r)$ term. In this exploratory study we also ignore any roche lobe overflow that may occur near periastron.

The relative velocity is given by

$$v_{rel}^2 = v_n^2 + v_w^2 - 2\mathbf{v}_n \cdot \mathbf{v}_w, \tag{4}$$

where v_w is Be star equatorial disk velocity, and v_n is the neutron star's orbital velocity. Combining equations (2) and (3) we obtain

$$\dot{\mathrm{M}}_n = \frac{4\pi (GM_n)^2 \rho}{v_{rel}^3}. \tag{5}$$

Thus $\dot{\mathrm{M}}_n$ depends directly on the local gas density and inversely on the cube of the relative velocity. In a highly eccentric orbit like that proposed for LS I +61°303, both the gas density and the relative velocity will vary significantly around the orbit. Since we are assuming $S \propto \dot{\mathrm{M}}_n$ then

$$S(r) = K(r) \frac{4\pi (GM_n)^2 \rho(r)}{v_{rel}^3(r)}, \tag{6}$$

or

$$k(r)\rho(r) = S(r) v_{rel}^3(r), \tag{7}$$

where

$$k(r) = K(r) 4\pi (GM_n)^2, \tag{8}$$

Thus knowledge of $S(r)$ and $v_{rel}(r)$ is sufficient to determine $k(r)\rho(r)$, where $K(r)$ is the unknown proportionality constant introduced in equation (1) and $\rho(r)$ is the equatorial disk density at r.

In equation (6), we explicitly assume that $S(r)$ is directly proportional to $\rho(r)$ and $v_{rel}^{-3}(r)$ at radius r, not the values at an earlier radius. This requires that any delay in the production of relativistic electrons from the accretion of disk gas at radius r, and in the transport of these relativistic electrons to a region where there synchrotron emission can escape to the observer, is negligible for the radial resolution we are employing for this analysis. If the disk is inclined sufficiently to the line of sight we may be able to view the particle generation region directly. Wood et al. (1997) deduced a disk half-opening angle of 2.5° for the Be star ζ Tau, from modeling the optical continuum spectropolarimetry. Thus Be star disks may be very thin. Hutchings and Crampton (1981) estimated the angle between the line of sight and the plane of the disk of LS I +61°303 at $15 - 20°$, based on their spectroscopic data. This combination might permit an unobscured line of sight to the relativistic particle acceleration region and provide a simple explanation for why the optical depth at 8.3 GHz is $<< 1$.

If there is no unobscured line of sight, the relativistic electrons must first propagate to optically thin regions above and below the plane of the disk, before radio emission can escape to the observer. At first glance this situation would appear to be at odds with the

observation that the optical depth of the 8.3 GHz radio emission is always << 1. However, if the particle production is continuous then there will always be a population of radiating electrons in the optically thin region, and this emission can dominate over emission from more opaque regions where the electrons are initially accelerated. Recent estimates from VLBI observations (Peracaula et al. 1998, Massi et al. 2001) indicate expansion velocities of the synchrotron emitting electrons ranging from of ~ 0.06 c to ~ 0.4 c. Using the lower of these estimates leads to a delay of only ~ 0.04 d to transport the relativistic electrons a distance equal to the major axis of the binary orbit.

Fig. 2 illustrates the geometry of the assumed orbit and the three velocities v_n, v_c, v_r involved in computing v_{rel}. The total Be star equatorial disk velocity v_w is given by $v_w^2 = v_c^2 + v_r^2$. For such an orbit v_n ranges from 511 km s^{-1} at periastron to 51 km s^{-1} at apastron. The spectroscopic observations indicate large values for v_c. For example, the Balmer lines show double-peak emission with peak separations of $\sim$ 440 km s^{-1} in H_β and $\sim$ 350 km s^{-1} in H_α (Gregory 1979, Hutchings and Crampton 1981, Zamanov et al. 2001). Hutchings and Crampton (1981) measured $v \sin i = 360 \pm 25$ km s^{-1} for the primary star. In addition, very broad H_α wings of $\sim$ 1100 km s^{-1} are observed, indicating larger Doppler broadening velocities than those of other B stars. Such profiles are, however, common in cataclysmic variables, in which a disk forms around a compact star whose Keplerian velocities extend to much greater values than main sequence or larger stars. If the high velocity emission is from a disk about the secondary then it should execute the orbital velocity of the secondary, however, Hutchings and Crampton (1981) were unable to find any direct evidence of emission from the secondary. Alternatively, the high velocity wings might indicate that the inner part of the disk co-rotates with the star, perhaps coupled by the star's magnetic field. Yet another possibility is non-coherent scattering, in which line photons are scattered into the line wings so they can escape from deeper layers in the disk where the source function is large, a long-known result from optically thick slabs (Hummel 2000).

The V/R ratio of the two emission line peaks is variable, but normally the long wavelength peak is stronger (as expected for a slow moving expansion). Hutchings and Crampton (1981) conclude that the star is undergoing mass loss through an equatorial disk with a high inclination ($\sin i \simeq 1$).

From equation (6) the observed flux density depends on the relative velocity of the neutron star and the wind. The relative velocity, v_{rel}, is given by

$$v_{rel}^2 = v_n^2 + v_c^2 + v_r^2 - 2v_n v_c \sin\phi - 2v_n v_r \cos\phi, \tag{9}$$

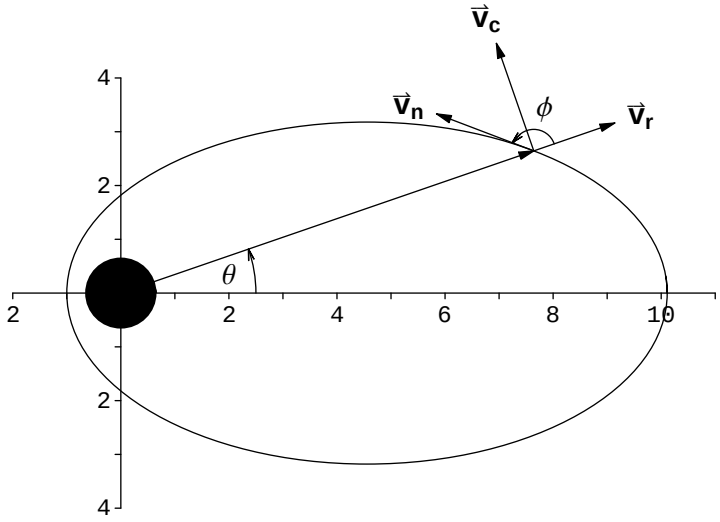

Fig. 2.— The orbit of LS I +61°303 drawn to scale illustrating the geometry used in the calculations.

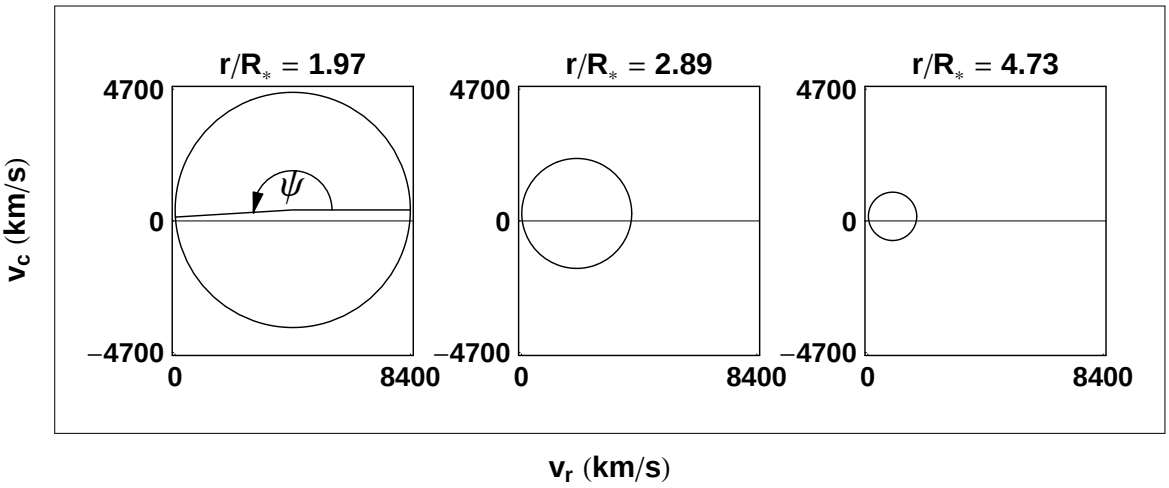

Fig. 3.— Sample solution loci for the radial and circular components of Be star equatorial disk velocity at three different radii.

where v_c is positive for counter clockwise rotation. The angle ϕ between the neutron star velocity and the radial component of the equatorial disk is given by

$$\phi = \frac{\pi}{2} + \arctan \frac{e \sin\theta}{1 - e\cos\theta} \tag{10}$$

Now consider two points on the neutron stars orbit at the same radius from the Be star. The first point is on the outbound portion of the orbit where the neutron star is traveling from periastron to apastron (out), and the second is on the ingoing portion of the orbit (in). Because both points have the same value of r, the density, $\rho(r)$, and magnitudes of $v_r(r)$ and $v_c(r)$ are the same. This follows from the circular symmetry assumption. The angle between v_n and v_c is the same for both points. What brakes the symmetry is the difference in angle between v_n and v_r at the two points. Thus if $v_r \neq 0$, then $v_{rel,out}(r) \neq v_{rel,in}(r)$ and hence $S_{out} \neq S_{in}$.

From the assumption of circular symmetry we can write

$$k(r)\rho(r) = S_{out}(r)\ v^3_{rel,out}(r) = S_{in}(r)\ v^3_{rel,in}(r) \tag{11}$$

From a knowledge of $S_{out}(r)$, $S_{in}(r)$, and $v_n(r)$ we can solve for a solution locus in v_r and v_c that satisfies equation (11). The solution locus, which is derived in the Appendix, can be written in the form

$$(v_r + \beta v_n \cos\phi)^2 + (v_c - v_n \sin\phi)^2 = (\beta^2 - 1) v_n^2 \cos\phi^2, \tag{12}$$

where

$$\beta = \frac{(\frac{S_{out}}{S_{in}})^{2/3} + 1}{(\frac{S_{out}}{S_{in}})^{2/3} - 1} \tag{13}$$

From the form of this equation we see that the solution is a circle in the v_r, v_c plane with radius $= \sqrt{(\beta^2 - 1)} v_n |\cos\phi|$, and center at $(-\beta v_n \cos\phi, v_n \sin\phi)$. We can parameterize the solution locus in terms of the angle ψ (see Fig. 3) between the radius vector from the center of the solution circle to a point on the locus and the direction of the positive v_r.

$$\begin{aligned} v_r(r) &= v_n(r)[\sqrt{\beta(r)^2 - 1}\ |\cos\phi(r)|\ \cos\psi - \beta(r)\ \cos\phi(r)] \\ v_c(r) &= v_n(r)[\sqrt{\beta(r)^2 - 1}\ |\cos\phi(r)|\ \sin\psi + \sin\phi(r)] \end{aligned} \tag{14}$$

Fig. 3 illustrates the solution locus for representative data at three different radii, corresponding to $r/R_* = 1.97, 2.89, 4.73$, where R_* is the radius of the Be star. The radius of the circle shows a strong dependence on r, the distance of the neutron star from the Be star. In general the observed values of $S_{out}(r)$ and $S_{in}(r)$ lead to solution loci in which v_r is positive

but v_c can be either positive or negative. Previous estimates of the outflow velocity at the surface of Be stars, based on the analysis of the infrared emission of equatorial disks (Waters 1986), are in the range $2 - 20$ km s^{-1}. The velocity radius of the solution locus, as shown in Fig. 3, varies from 4195 km s^{-1} at $r/R_* = 1.97$ to 122 km s^{-1} at $r/R_* = 14.9$. Thus only a small fraction of each solution locus is likely to be physically meaningful, corresponding to values of ψ in the vicinity of $\psi = \pi$.

3. Radial Distributions of $v_r(r)$ and $k(r)\rho(r)$

The velocity of gas in the Be star equatorial disk wind can be decomposed into $v_c(r)$ and $v_r(r)$. In this section we derive $v_r(r)$ and $k(r)\rho(r)$ for all of the 8.3 GHz data assuming different models for $v_c(r)$. The steps on the calculation are as follows.

1. The data consists of daily average flux densities as a function of time, $S(t)$, expressed as a Julian Day (JD) number. The first step is to translate our origin of time to a JD corresponding to periastron passage. Call this JD$_{peri}$. The GBI data spans roughly 1.5 P_2 cycles so we chose a JD$_{peri}$ close to the start of the first of these P_2 cycle. We used the radio phase of periastron passage (0.4) given in paper III to arrive at JD$_{peri} = 2,449,471.5$. The data were then converted to an orbital time according to

$$t_{orb} = \left(\frac{(t - \mathrm{JD_{peri}})}{P_1} - \mathrm{IntegerPart}[\frac{(t - \mathrm{JD_{peri}})}{P_1}] \right) P_1 \tag{15}$$

2. Each orbit was then divided into two halves, one corresponding to the outbound portion of the neutron's star orbit and the other to the inbound phase of the orbit. For each half the values of t_{orb} were converted to values of r in two steps. First they were converted to orbital phases, θ, by solving the differential equation

$$\frac{d\theta[t_{orb}]}{dt} - \sqrt{\frac{G(M_{Be} + M_N)}{a^3(1-e^2)^3}}(1 - e\ Cos[\theta])^2 = 0, \tag{16}$$

assuming the initial condition $\theta[0] = \pi$ radians at periastron. Here e = the orbital eccentricity and a = the semi-major axis which is given by Kepler's third law.

$$a = \left(\frac{P_1^2 G(M_{Be} + M_N)}{4\pi^2} \right)^{1/3}. \tag{17}$$

These orbital phases were converted to orbital radii, r, from the geometry of an ellipse.

$$r[\theta] = \frac{a(1-e^2)}{1 - e\ \cos[\theta]} \tag{18}$$

3. What we are after are pairs of $S_{out}(r)$ and $S_{in}(r)$ with the same value of r on the outbound and inbound portions of each orbit. The daily measurements of flux density did not always provide flux pairs at the same value of r, so it proved necessary to linearly interpolate the measured values onto a finer grid in r before pairing. These flux density pairs together with the P_2 phase of the midpoint of the orbit, computed assuming $P_2 = 1667$ days, were the fundamental data for the remainder of the analysis.

4. Values of v_r were then computed for 15 uniformly spaced values of r, from the $S_{out}(r), S_{in}(r)$ pairs and equations (13) and (14), assuming a specific model for v_c.

5. We computed values of $k(r)\rho(r)$ from equations (7), (9), and (10), for the same 15 uniformly spaced samples of r.

These calculations were carried out for the two different averages of the data. In the first case (a), we are after the average properties of the disk versus radius where we are averaging over all P_2 phase. In the second case (b), we divide the data into 9 P_2 phase bins and examine the average disk properties as a function of radius within these phase bins and the fractional change in density from that found from the average in case (a).

3.1. Average disk properties

Fig. 4 shows the average outbound and inbound flux densities versus radius for the entire Green Bank Interferometer data set which spans approximately 1.5 P_2 cycles.

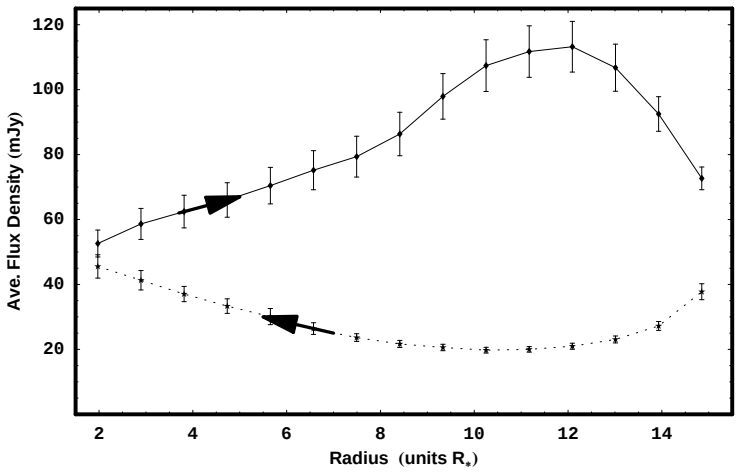

Fig. 4.— The average outbound and inbound flux densities in 15 orbital radii bins.

The solution loci illustrated in Fig. 3 allows us to set limits on the minimum $v_r(r)$ at any given radius. We obtain the minimum value of $v_r(r)$ and the corresponding $v_c(r)$, from equations (14), by setting $\psi = \pi$. The value of β used to compute $v_r(r)$ in equation (14) is computed from the ratio of S_{out}/S_{in} at any particular radius for all of the data. We will refer to these as the velocity components at minimum $v_r(r)$, and designate them by $[v_r(r), v_c(r)]_{mvr}$. Other solutions for $v_r(r)$ can be obtained from the solution loci by adopting different models for $v_c(r)$ that have been proposed in the literature. The other models considered for $v_c(r)$, which are discussed below, are designated Zero, Keplerian, Mennickent, and Co-rotate. The $[v_r(r), v_c(r)]$ solutions for these models are compared to the $[v_r(r), v_c(r)]_{mvr}$ solutions in panels (a) and (b) in Fig. 5.

Panel (a) of Fig. 5 shows that $[v_r(r)]_{mvr}$, as indicated by the curve labeled mvr, first increases with radius out to $r/R_* \sim 6$, then exhibits a broad maximum between $r/R_* \sim 6-12$ around a value of 25 km s^{-1}, and drops rapidly beyond. At the inner radius this analysis probes ($r/R_* \sim 2$) we obtain $[v_r(r)]_{mvr} \sim 5$ km s^{-1}.

Examination of equation (14) indicates that for $\psi = \pi$, $v_c(r)$ is given by

$$v_c = v_n \sin\phi, \tag{19}$$

i.e., the circular component of the Be star equatorial disk velocity is equal to the azimuthal component of the neutron star's velocity. Thus the disk radial velocity is a minimum when the relative circular motion of the wind and neutron star is zero. Since the angular momentum of the neutron star is conserved we have that the $[v_c(r)]_{mvr} \propto r^{-1}$. This $1/r$ dependence is indicated by the line in panel (b) labeled "mvr".

Extrapolating the curve labeled $[v_r]_{mvr}$ of Fig. 5(a) to the surface of the Be star indicates an initial outflow velocity of v_r of a few km s^{-1}. This falls in the range of initial outflow velocities computed for the Be star equatorial disk in LS I +61°303 by Martí and Paredes (1995), and is typical of Be star equatorial disk outflow velocities in general (Waters 1986). This would suggest that perhaps $[v_c(r)]_{mvr}$ is a good estimate of the circular component, $v_c(r)$, of the gas velocity. It is interesting to note that this choice of circular velocity would result in a minimum drag force on the neutron star. Unfortunately when we extrapolate $[v_c(r)]_{mvr}$ to the surface of Be star, $r/R_* = 1$, we obtain a value of 773 km s^{-1} which exceeds the escape velocity for the Be star of $\simeq 617$ km s^{-1}. In contrast the Keplerian orbital speed at the surface is $\simeq 436$ km s^{-1}.

The solution loci also allow us to set limits on the maximum $v_c(r)$ at any given radius obtained by setting $\psi = \pi/2$ in equation (14). The corresponding values of $v_r(r)$ are very large reaching values of ~ 4200 km s^{-1} at small radii. The plot of maximum $v_c(r)$ versus radius is labeled "Mvc" in Fig. 5(b). The maximum $v_c(r)$ curve is useful because it allows

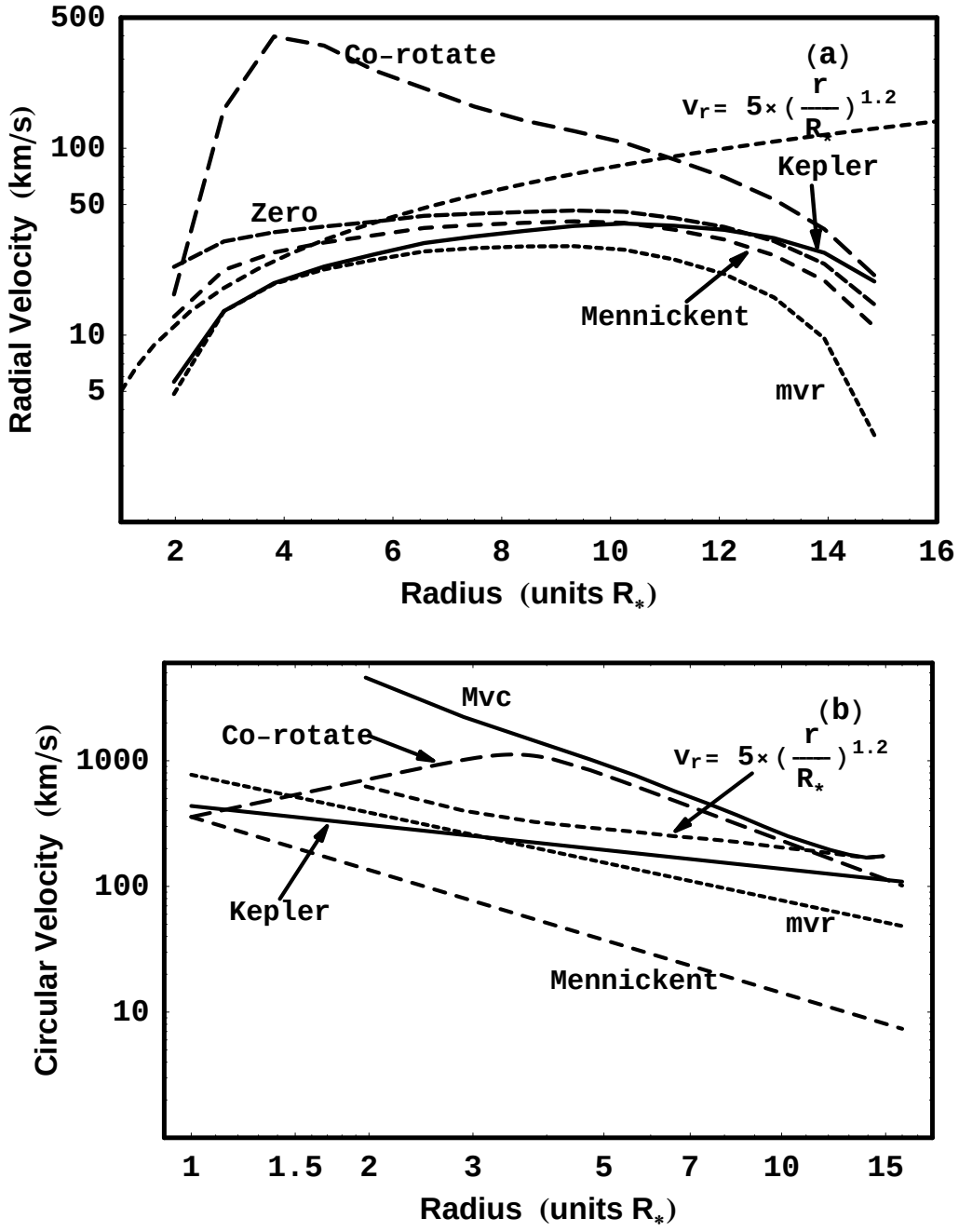

Fig. 5.— Panel (a) shows $v_r(r)$ for five different models of $v_c(r)$, as discussed in the text, together with $v_r(r) = 5(r/R_*)^{1.2}$ from Marti and Paredes (1995). Panel (b) shows the five different models of $v_c(r)$ plus an upper limit on $v_c(r)$ which is designated Mvc. We also show our derived $v_c(r)$ relation corresponding to the $v_r(r) = 5(r/R_*)^{1.2}$.

us to constrain any disk model that proposes an inner region that co-rotates with the star. One example of this is the magnetically confined wind shock (MCWS) model of Babel and Montmerle (1997), originally proposed to account for the X-ray and radio emission from Ap-Bp stars. Donati et al. (2001) applied this model to β Cep, a pulsating star with recurrent Be episodes. The existence of an inner co-rotating region would provide one way to account for the ~ 1100 km s^{-1} breadth of the H$_\alpha$ emission lines. The large dash curve in Fig. 5(b) corresponds to a co-rotating disk model ("Co-rotate") with $v_c(R_*) = v_* = 360$ km s^{-1} (see discussion of v_* below). This reaches a maximum $v_c(r)$ of $\simeq 1100$ km s^{-1} at a radius of $\sim 3.5R_*$. To stay within the upper limit of $v_c(r)$, designated by curve Mvc, $v_c(r)$ for a co-rotation model must decline rapidly beyond the co-rotating region. The Co-rotate curve in Fig. 5(b) has an $r^{-1.75}$ dependence at large radii which is a much steeper fall off than a Keplerian $r^{-0.5}$.

Another model for $v_c(r)$ that we examined comes from the work of Mennickent et al. (1994). They analyzed the rotational properties of Be star envelopes based on the equivalent widths and peak separation of H$_\alpha$ emission. They assumed a power law rotation of the envelope and obtained a best fit for

$$v_c(r) = v_* \ (r/R_*)^{-1.4}, \tag{20}$$

where v_* is the equatorial stellar rotation velocity which we set $= 360$ km s^{-1} from the measured $v \sin i = 360$ km s^{-1} and the fact that $\sin i \sim 1$. Compared to the computed Keplerian orbital speed at the stellar equator of $v_{Kep} = 436$ km s^{-1}, we find that $v_* \simeq 0.83 v_{Kep}$. Equation (20) for $v_c(r)$ is labeled "Mennickent" in Fig. 5(b) and the corresponding curve for $v_r(r)$ is given in Fig. 5(a). In general for each model of $v_c(r)$ there are two solutions to $v_r(r)$, the larger of which is physically unreasonable based on the discussion above and is ignored.

We also considered a Keplerian model of the form $v_c(r) = \sqrt{GM_{Be}/r}$. The curves for $v_c(r)$ and the corresponding $v_r(r)$ are labeled "Kepler" in Fig.s 5(b) and (a), respectively. The values of $v_r(r)$ obtained for this model remain close to the $[v_r(r)]_{mv}$ values at small radii.

The behavior of $v_r(r)$ for the co-rotating disk model is markedly different from the other models mentioned so far. The values of $v_r(r)$ are an order of magnitude larger, with the maximum occurring at the outer edge of the inner co-rotation region. If the boundary of the co-rotation region is determined by the magnetic field we might expect $v(r)$ to be larger outside the co-rotation region, i.e., opposite to what is indicated.

Martí and Paredes (1995) deduced a radial outflow velocity law from a power law wind density $\rho \propto r^{-n}$ model used in fitting their near infrared data of LS I +61°303. For a constant outflow rate the continuity equation leads to a radial outflow of the form $v_r(r) \propto r^{n-2}$.

Adopting an initial $v_r = 5$ km s^{-1} and their best fit $n = 3.2$, they arrived at the equation $v_r(r) = 5 \times (r/R_*)^{1.2}$ km s^{-1}. This equation is plotted and labeled in Fig. 5(a). We have combined their model for $v_r(r)$ with our velocity solution loci and derived the $v_c(r)$ law that corresponds to their $v_r(r)$ model. This is plotted and labeled in Fig. 5(b). The curve starts off parallel to the mvr model (angular momentum conservation) at small radii and then ends up parallel to the Keplerian solution at larger radii. Extrapolating the curve back to $r = R_*$ yields a $v_c \sim 1300$ km s^{-1}, i.e. much larger than the escape velocity. We tried lowering the initial value of v_r but that exaggerated the kink (slope change) in the $v_c(r)$ curve. This may indicate problems with assuming a simple power law for $\rho(r)$ in the analysis of the near infrared data.

Fig. 5(a) can also be used to set a lower limit on any model of the form $v_r(r) =$ a constant velocity. This velocity must exceed the maximum of the $[v_r]_{mvr}$ curve which is ≈ 25 km s^{-1}.

Finally it is of interest to see what $v_r(r)$ behavior corresponds to a $v_c(r) = 0$ model. This curve is labeled "Zero" in Fig. 5(a).

Fig. 6(a) shows the behavior of $k(r)$ $\rho(r)$ for the Mennickent, Kepler and mvr wind velocity models, calculated from equations (11) and (9) together with $S_{out}(r)$. Of course if $k(r)$ was a simple constant independent of r, then the curves in Fig. 6(a) would indicate the radial dependence of the disk density.

We expect, however, that $k(r)$ is not a constant especially at small radii for the following reason. The work of Taylor et al. (1992) and Martí and Paredes (1995) indicates that two accretion maxima will occur, one at periastron and a second on the outbound portion of the neutron stars orbit. Relativistic electrons produced near periastron will suffer severe inverse-Compton losses from scattering off photons in the radiation field of the primary giving rise to X-ray and $\gamma-$ray energies. Thus near periastron we expect an X-ray and possible gamma-ray outburst but very little in the way of radio emission. The limited X-ray observations available do exhibit a maximum around periastron. For the second accretion peak the neutron star is further from the primary and inverse-Compton losses will be much less. If this picture is correct, we expect a smaller fraction of the gravitational energy released in accretion to appear in the form of radio emission near periastron than at larger radii. This implies that $k(r)$ will be smaller near periastron. We explore this issue further in the next section.

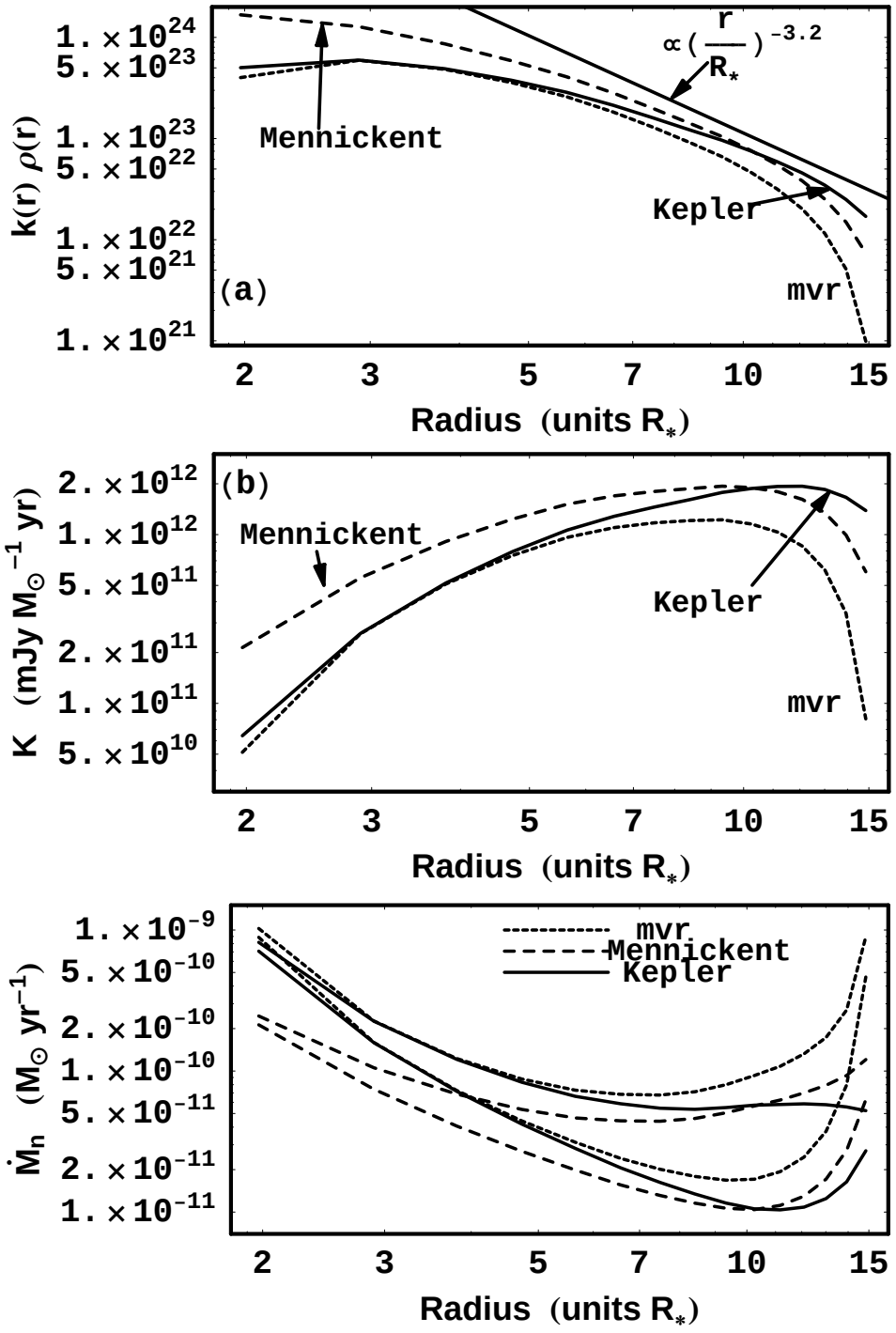

Fig. 6.— Panel (a) (b) and (c) show the radial dependence of $k(r)\rho(r)$, $K(r)$ and $\dot{\mathrm{M}}$ respectively, for three different models of $v_c(r)$.

3.2. Estimating the neutron star accretion rate

We can combine our estimate of $k(r)\ \rho(r)$ in Fig. 6(a) with independent estimates of $\rho(r)$ to estimate $k(r)$. In their analysis of the infrared excess of LS I +61°303, Waters et al. (1988) assumed a power law radial density dependence of the form

$$\rho(r) = \rho_0 (r/R_*)^{-n}, \tag{21}$$

and obtained $n = 3.25$ and $\log \rho_0 = -10.6$ (g cm^{-3}), with $R_* = 10 R_\odot$. Martí and Paredes (1995) obtained a very similar result of $n = 3.2$ and $\log \rho_0 = -11.0$ (g cm^{-3}).

If the power law assumption for $\rho(r)$ is valid then we can derive $k(r)$ from a comparison of our results for $k(r)\ \rho(r)$ to equation (21), adopting the more recent results of Martí and Paredes (1995) for ρ_0 and n. From $k(r)$ we can compute $K(r)$ from equation (8). The derived $K(r)$ for three of the models, which is shown in Fig. 6(b), exhibits a maximum of $\sim 10^{12}$ mJy M$_\odot^{-1}$ yr at $r/R_* \simeq 11$. The value of $K(r)$ exhibits a decrease at both small and large values of r. The decrease at small r might reflect the relative importance of inverse-Compton losses over synchrotron losses at small radii. Another possible reason for a drop in $K(r)$ at small radii, is a break down in the assumption of spherically symmetric accretion if the disk thickness is $< r_{acc}$. The decrease at large values of r may indicate a break down in the assumed power law approximation for $\rho(r)$ at a radius $> 11 \times R_*$, and suggests a much more rapid decline in disk density at larger radii.

We have estimated the mass accretion rate of the neutron star, $\dot{\mathrm{M}}_n$, from equation (1) using the derived $K(r)$ and the measured values of $S_{8.3}(r)$ averaged over all P_2 phase. This is shown in Fig. 6(c). As expected there is a large variation in $\dot{\mathrm{M}}_n$ around the orbit. A typical value of $\dot{\mathrm{M}}_n$ is $\sim 10^{-10}$ M$_\odot$ yr^{-1}. For comparison, the mass outflow rate in the Be star disk is estimated to be in the range $0.4 - 4.0 \times 10^{-7}$ M$_\odot$ yr^{-1} (Martí and Paredes 1995).

For all three models of $v_c(r)$, $\dot{\mathrm{M}}_n$ increases towards periastron reaching values close to $\sim 10^{-9}$ M$_\odot$ yr^{-1} at an $r/R_* = 2$ for two of the models. For the Kepler model a secondary accretion peak can be seen around $r/R_* \simeq 11$. For the other two models the accretion simply rises again towards apastron. The variation in $\dot{\mathrm{M}}_n$ with radius ranges from a factor of ~ 25 for the Mennickent $v_c(r)$ model to a factor of ~ 80 for the Kepler model.

It is useful to compare $\dot{\mathrm{M}}_n$ to the Eddington accretion limit for a neutron star which is $\sim 10^{-8}$ M$_\odot$ yr^{-1}. For the Mennickent circular velocity model, $\dot{\mathrm{M}}_n$ corresponds to the range ~ 0.001 to $\sim 0.01\ \dot{\mathrm{M}}_{\mathrm{Eddington}}$. This translates to an expected luminosity range of $\sim 10^{35}$ to $\sim 10^{36}$ ergs s^{-1} which is comparable to estimates of the total X-ray and γ-ray luminosity for LS I +61°303.

3.3. Phase bin averages

In this section we divide the data into 9 P_2 phase bins and examine the average disk properties as a function of radius within these phase bins and the fractional change in density from that found from the average in Section 3.1. For this analysis to be valid we require circular symmetry when averaging over approximately 7 orbits or ~ 185 days. One of our 9 P_2 phase bins contained only one data point so only the results for 8 bins are illustrated in Fig.s 7 to 10 below.

The above calculations were carried out for four models of $v_c(r)$: (a) $[v_c(r)]_{mvr}$ (minimum v_r model), (b) $v_c(r) = \sqrt{GM_{Be}/r}$ (Keplerian model),(c) $v_c(r) = v_*\ r^{-1.4}$ (Mennickent et al. 1994), and (d) model Co-rotate, with an inner co-rotating region. The results for cases (a), (b), (c), and (d), are shown in Fig.s 7, 8, 9, and 10, respectively. Column (a) in each figure gives the mean and standard deviation of the derived values of v_r for 8 different P_2 phase bins. The second column gives similar information for the product $k(r)\ \rho(r)$. The third panel gives $\Delta\rho_f(r)$ = the percent change in $k(r)\ \rho(r)$ from $[k(r)\ \rho(r)]_{ave}$, the average value of $k(r)\ \rho(r)$ at radius r, where the average is taken over all P_2 phase. This is discussed in Section 4.

4. Changes in Disk Density Versus P_2 Phase

Even if we do not know $v_c(r)$, we can still extract very useful information concerning the fractional change in $\rho(r)$, provided $k(r)$ is constant in time at any particular radius. For example if the Be star were to eject an outward moving shell of gas this would give rise to a modulation in ρ at any fixed radius. Let $\rho(r,t)$ = the density at time t.

$$k(r)\rho(r,t) = S_{out}(r,t)v^3_{rel,out}(r,t) \tag{22}$$

For any particular value of t, different points on the solution locus for $v_r(r), v_c(r)$ lead to different values for $k(r)\rho(r,t)$. Now consider $\Delta\rho_f(r,t)$ = the fractional change in $k(r)\rho(r,t)$ from $[k(r)\ \rho(r)]_{ave}$, the average value of $k(r)\ \rho(r)$ at radius r, where the average is taken over all P_2 phase.

$$\Delta\rho_f(r,t) = \frac{k(r)\ \rho(r,t) - [k(r)\ \rho(r)]_{ave}}{[k(r)\ \rho(r)]_{ave}} = \frac{S_{out}(r,t)\ v^3_{rel,out}(r,t) - [S_{out}(r)\ v^3_{rel,out}(r)]_{ave}}{[S_{out}(r)\ v^3_{rel,out}(r)]_{ave}}, \tag{23}$$

If $k(r)$ is independent of time then this factor cancels out and equation (23) reduces to

$$\Delta\rho_f(r,t) = \frac{\rho(r,t) - [\rho(r)]_{ave}}{[\rho(r)]_{ave}}. \tag{24}$$

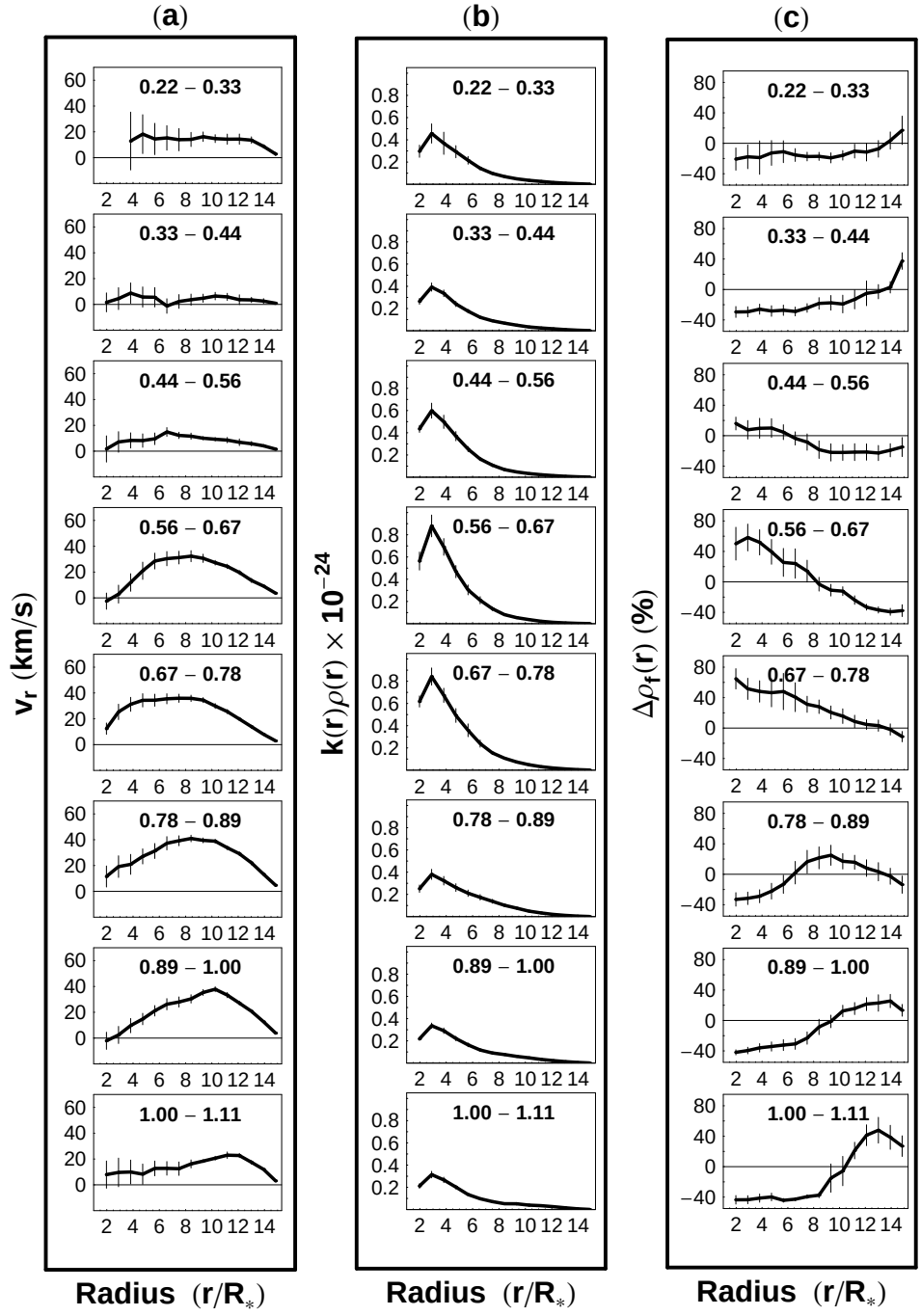

Fig. 7.— The three panels show the derived values of (a) the radial component of gas velocity, $v_r(r)$, (b) $k(r)\ \rho(r)$, and (c) $\Delta\rho_f(r)$, the percentage change in the gas density from the average, for 8 P_2 phase bins, assuming the **minimum v_r velocity model**.

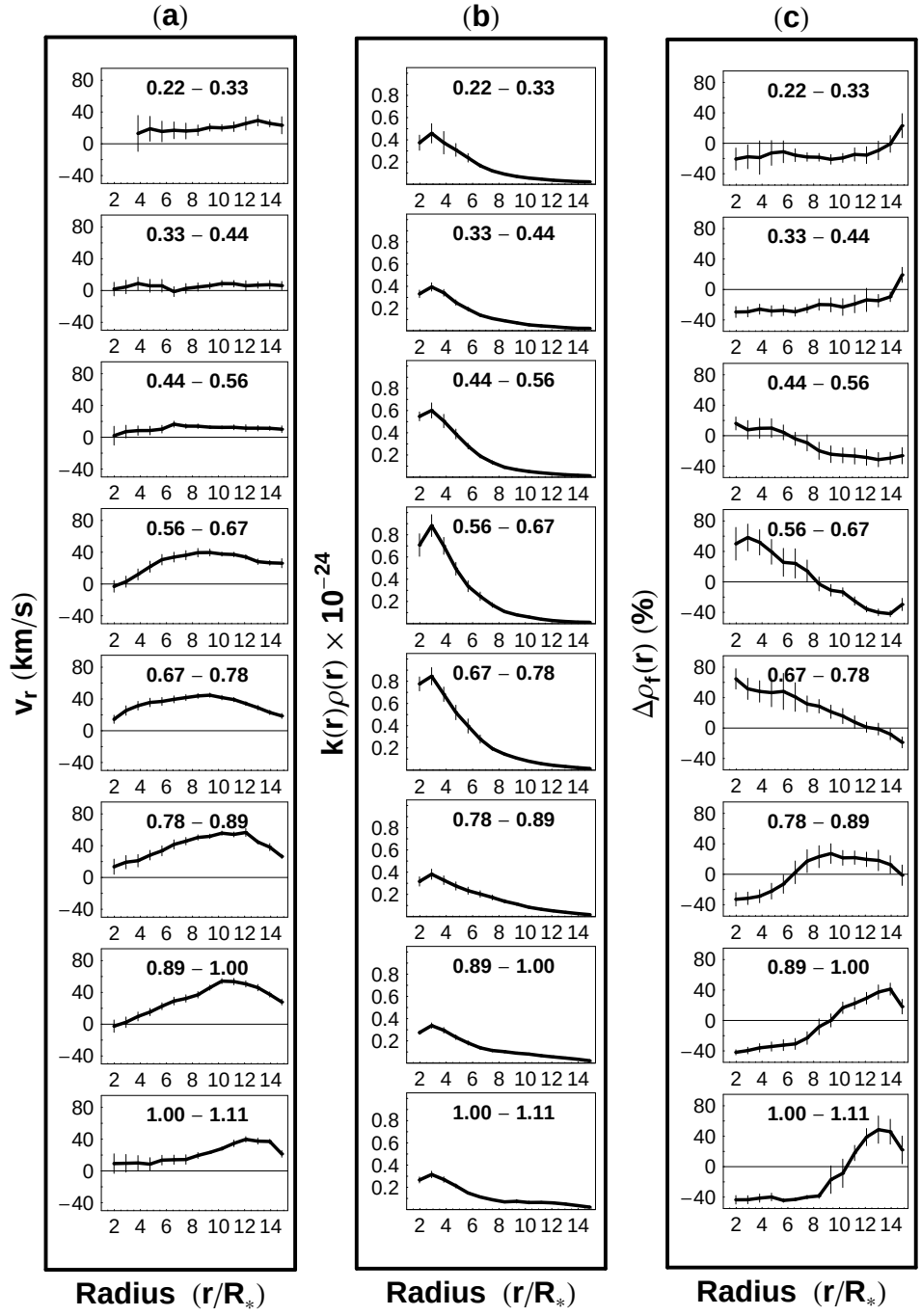

Fig. 8.— The three panels show the derived values of (a) the radial component of gas velocity, $v_r(r)$, (b) $k(r)\ \rho(r)$, and (c) $\Delta\rho_f(r)$, the percentage change in the gas density from the average, assuming a **Keplerian circular velocity model**.

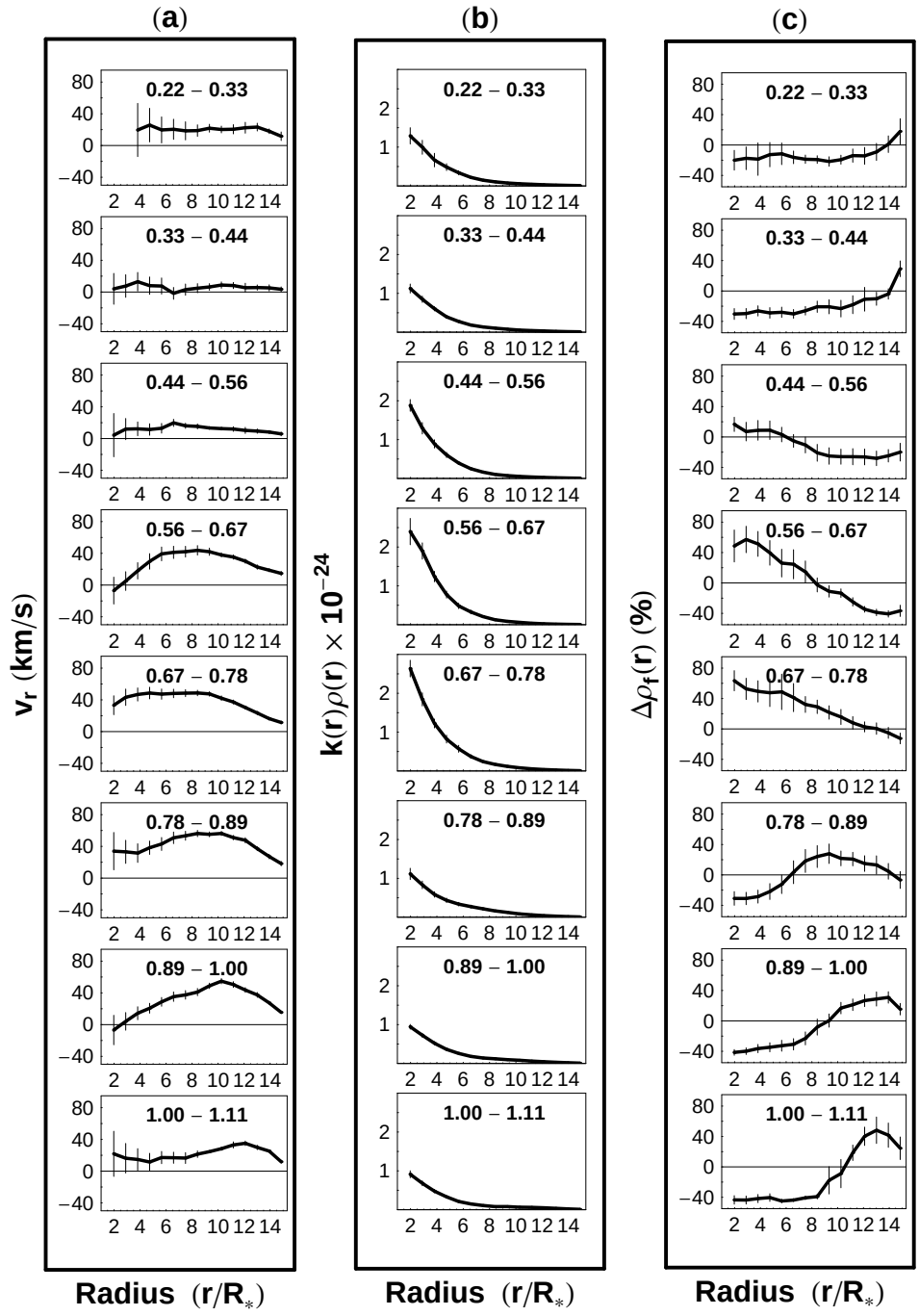

Fig. 9.— The three panels show the derived values of (a) the radial component of gas velocity, $v_r(r)$, (b) $k(r)\ \rho(r)$, and (c) $\Delta\rho_f(r)$, the percentage change in the gas density from the average, assuming the **Mennickent et al. (1994) circular velocity model**.

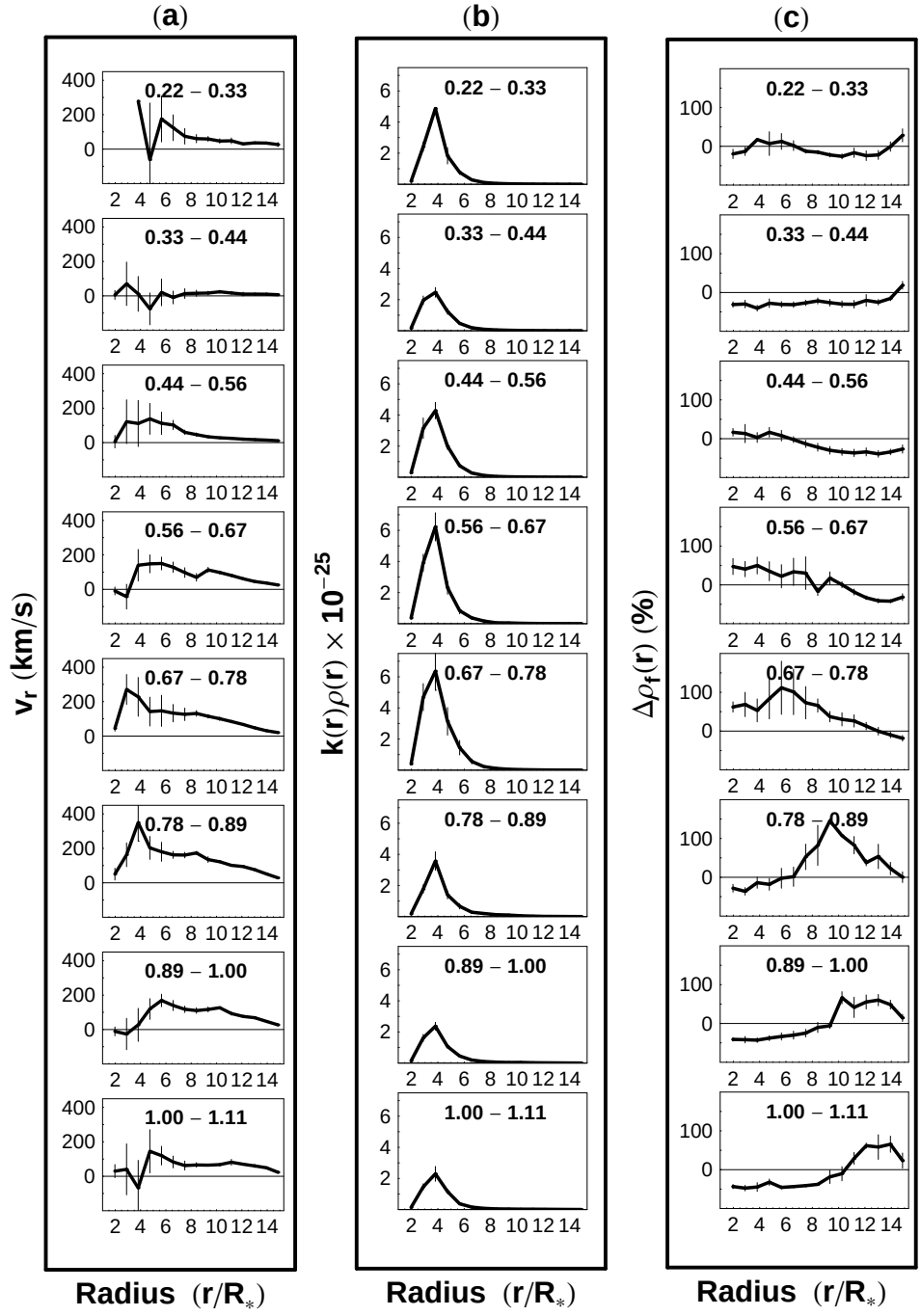

Fig. 10.— The three panels show the derived values of (a) the radial component of gas velocity, $v_r(r)$, (b) $k(r)\ \rho(r)$, and (c) $\Delta\rho_f(r)$, the percentage change in the gas density from the average, assuming **model Co-rotate, with an inner corotating region**.

Equations (23) and (24) predict that if $k(r)$ is independent of time then the quantity

$$\frac{S_{out}(r,t)\ v^3_{rel,out}(r,t) - [S_{out}(r)\ v^3_{rel,out}(r)]_{ave}}{[S_{out}(r)\ v^3_{rel,out}(r)]_{ave}}$$

will be the same for all points on the solution locus for $v_r(r), v_c(r)$. If this proves to be true then it is extremely useful property of the fractional change in $S_{out}\ v^3_{rel,out}$. Further it does not require k to be the same at all radii. Thus although we cannot uniquely determine the density at any one time, we might be able to uniquely determine the fractional change in density as a function of time and thus study the evolution of disk density radial profile.

In practice we computed the average (at each radius) of $\Delta\rho_f(r,t)$, over a series of orbits which fall in a particular P_2 phase bin, since we are interested in the dependence on the disk properties with P_2 phase. This new average is labeled $\Delta\rho_f(r)$ without the t dependence.

So the test is to see if we obtain the same values of $\Delta\rho_f(r)$ for our different choices of $v_c(r)$ models. In practice we stumbled on this property by accident. We first computed $\Delta\rho_f(r)$ versus P_2 phase, assuming $v_c(r) = 0$. We repeated the procedure for the four models of $v_c(r)$ discussed above. In all five cases we obtained the same $\Delta\rho_f(r)$, within the uncertainties. In contrast the P_2 phase behavior of $k(r)\ \rho(r)$ differs significantly over the range of $v_c(r)$ models. The third column of plots in Fig.s 7, 8, 9, and 10 shows $\Delta\rho_f(r)$ for the four $v_c(r)$ models mentioned above, for 9 different P_2 phase bins. One of the phase bins, $P_2 = 0.11 - 0.22$ contained only one data value and is thus not shown. The fact that they are all essentially identical, appears to confirm that $k(r)$ is a constant in time at any given radius and therefore that $\Delta\rho_f(r)$ is a good measure of the percentage change in the gas density from the average at that radius.

The evolution of $\Delta\rho_f(r)$ with P_2 phase clearly indicates an outward moving density enhancement which is first detected at small radii in the P_2 phase bin 0.44-0.56. By the next P_2 phase bin the build up reaches a maximum of $\sim 60\%$ and extends to around $r \simeq 8 \times R_*$. The location of the peak progresses steadily outwards. By P_2 phase ~ 1.05 the peak is very close to the outer limit of our detection radius of $15 \times R_*$ or $\simeq 1.05 \times 10^{13}$ cm. The peak is followed by a drop in $\Delta\rho_f(r)$ which is deepest at large radii about the time a new positive enhancement is occurring at small radii (see P_2 phase bin 0.44-0.56).

To estimate the radial velocity of the shell or density enhancement, we computed the weighted mean radius of the region exhibiting positive values of $\Delta\rho_f(r)$, for each phase bin. The weight assigned at each radius was simply the value of $\Delta\rho_f(r)$ at that radius. These measurements of mean radius versus P_2 phase, together with the best fit straight line, are shown in Fig. 11. For $P_2 = 1667$ days, the results are consistent with a constant radial velocity of 1.0 ± 0.13 km s^{-1}. Extrapolating back to the radius of the Be star, we conclude

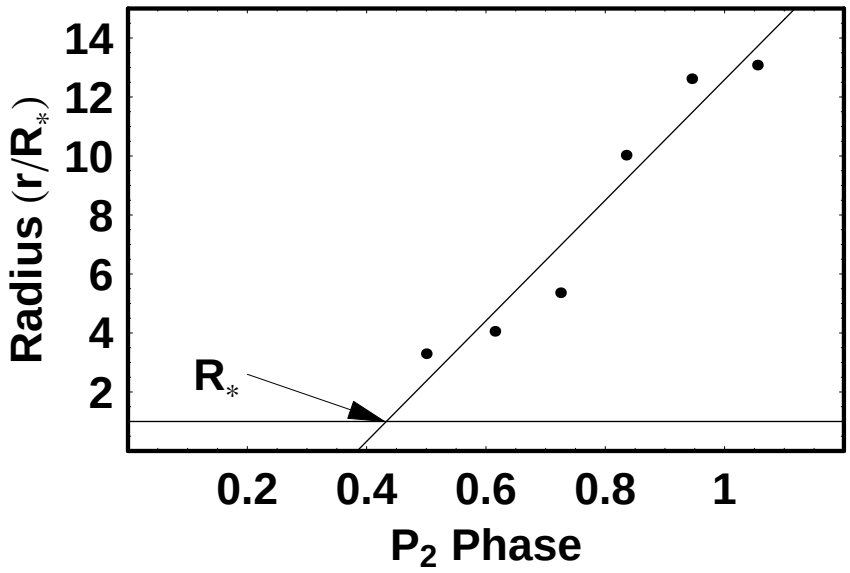

Fig. 11.— The weighted mean radius of the positive enhancement in $\Delta\rho_f(r)$ versus P_2 phase. The intersection of the best fitting line with R_*, the radius of the Be star, is indicated by an arrow.

that ejection process begins at P_2 phase $= 0.43 \pm 0.05$. The density enhancement first becomes detectable when it reaches periastron around P_2 phase $= 0.46$. It is somewhat surprising that the derived shell velocity is approximately a factor of 10 smaller than the typical radial component of the gas velocity. However, at this time we still do not understand the mechanism that forms and maintains the disk. Hopefully the present result will provide a valuable clue. Perhaps the disk enhancement corresponds to the motion of a slowly moving standing wave pattern.

The scale and general behavior of $v_r(r)$ in Fig.s 7, 8, and 9, corresponding to three of the $v_c(r)$ models, are approximately the same. All three figures demonstrate that $v_r(r)$ is a minimum in the P_2 phase bin 0.33-0.44, just prior to the onset of a new ejection cycle. After the ejection commences the values of $v_r(r)$ increase considerably reaching levels of $\sim 40 - 50$ km s^{-1}, with evidence for the radius of the peak in $v_r(r)$ loosely correlating with the location of the peak in $\Delta\rho_f(r)$.

The behavior of $v_r(r)$ for the co-rotating disk model is markedly different from the other models. The values of $v_r(r)$ are an order of magnitude larger, with the maximum always occurring at the outer edge of the inner co-rotation region. If the boundary of the co-rotation region is determined by the magnetic field we might expect $v(r)$ to be larger

outside the co-rotation region, i.e., opposite to what is indicated. For none of the models do we find evidence for any systematic negative velocities which would suggest gas returning to the star.

5. Discussion

The results of this exploratory study indicate that the $\sim$ 4.6 yr modulation in radio properties may stem from periodic ejections of a shell (density enhancement) of gas in the equatorial disk of the Be star. The calculations are based on the orbital parameters given in section (2). Martí and Paredes (1995) found that $M_* = 18M_\odot, R_* = 16R_\odot$ and $e = 0.7$ gave a reasonable fit to their infrared data as well, so we re-did our calculations with this combination, leaving the other parameters the same. Qualitatively our conclusions are unaltered by this change, and in particular, the same expanding density shell is observed in $\Delta\rho_f(r)$, the difference is that inner and outer radii are now $1.8 \times R_*$ and $10.7 \times R_*$, respectively.

It is interesting to compare the outward moving density enhancement in the equatorial disk with the recent results of Zamanov and Martí (2000) on the EW(H_α) and $\Delta V_{\rm peak}$. When we correct their P_2 phase to the latest value of $P_2 = 1667$ days (Gregory 2002), their minimum EW(H_α) and maximum $\Delta V_{\rm peak}$ occur at a P_2 phase = 0.65, and their maximum EW(H_α) and minimum $\Delta V_{\rm peak}$ occur at a P_2 phase = 0.19. The former is closest to our estimate of the launch of a new shell and the latter corresponds roughly to the phase at which the shell reaches apastron (see Fig. 10). According to Marlborough et al. (1997) the H_α in the disk of another Be star, ψ Persei, is optically thick. In such a situation an increase in radius of the shell would yield a stronger line and a lower $\Delta V_{\rm peak}$ as observed. This assumes that $v_c(r)$ decreases with radius. It is also clear from the results of Zamanov and Martí (2000), that the equatorial disk never completely disappears for H_α is detected at all P_2 phases. Our maximum fractional density change is from -40% to $+60\%$ which is also consistent with the idea that the disk never completely disappears.

In this exploratory analysis we have assumed the disk is circularly symmetric. While this is a reasonable assumption when we average over all P_2 phase, it might not be valid for individual orbits or for time intervals that are small compared to P_2. For example, Vakili et al. (1998) detected a prograde rotating one-armed density wave in the disk of the Be star ζ Tauri, based on sub-mas interferometry. The rotation of one-armed density wave in Be star disks provides an explanation for cyclic variations in the H_α V/R ratios that are observed in some Be stars. ζ Tauri exhibits a 3.1 year periodic oscillation in the H_α V/R ratio. To date there is no claim of periodic variations in the H_α V/R ratio for LS I $+61°303$.

Could such a process be responsible for the 4.6 periodic modulation in LS I +61°303? In their paper Vakili depict the one-armed density wave as a one-sided bar of enhanced density which rotates. Such a bar could account for the progressive outburst orbital phase delay observed for the portion of P_2 that the bar intersects the outbound portion of the neutron star orbit. Once the bar passes apastron we would expect the outbursts to be become (a) weaker or (b) disappear, depending on how large the bar density enhancement is compared to the rest of the disk.

In case (a) the outburst phase shift should continue to increase to a maximum of one, which is at odds with the maximum phase shift observed of ~ 0.5 (Gregory 2002). In case (b) they should disappear for half of a P_2 cycle and for the half of the orbit that they are observable the total phase shift should be 0.5. The latest results indicate that the outbursts become weaker for approximately half of a P_2 cycle but the phase of the weaker outbursts are still discernible (see Fig. 4 of Gregory 2002). For the half of the P_2 cycle for which the outbursts are strong the total phase shift is only 0.25 which is at odds with the predictions of a one-armed density wave model. Thus the one-armed density wave model does not agree quantitatively with the measurements for LS I +61°303.

There are two other important questions that remain unanswered. Firstly, what triggers the periodic shell ejections, and secondly, what gives rise to the disk geometry? What light does our new analysis shed on these questions? One possibility is that there is some resonance effect occurring between the neutron star and B star. We propose one worth further investigation. There has been considerable discussion in the literature (e.g. Zamanov 1995, Gregory et al. 1999, Zamanov et al. 2001) about possible transitions in the interaction of the neutron star and the Be star disk from an accretor propellor phase to an ejector phase following the theory of the gravimagnetic rotator (Lipunov 1992). We suppose for most of the P_2 cycle, the neutron star is in the accretor propellor phase, and that the propellor action of the magnetosphere results in particle acceleration which gives rise to the synchrotron radio emission. After the shell expands beyond apastron the density drops low enough near apastron that a brief transition is made to the ejector phase around $P_2 \simeq 0.4$. A relativistic wind is launched, which upon interacting with the rapidly rotating B star, triggers a new shell ejection which quenches the ejector phase. This phase might be identified by the brief appearance of a radio pulsar.

While the exact mechanism responsible for the creation of Be star equatorial disks is still unknown, several models have been put forward in an attempt to explain the phenomenon. The first is known as the wind compressed disk (WCD) model. Developed by Bjorkman and Cassinelli (1992), the model postulates that the characteristically rapid rotation of Be stars is responsible for the presence of a disk. A gas particle in the stellar wind from a rapidly

rotating star will enter a tilted orbit. Eventually material from opposite hemispheres will collide at the equator, causing a disk of compressed gas to form. This model requires a high stellar rotational velocity consistent with the measured $v \sin i$ for LS I +61°303.

Another possibility is the magnetically confined wind shock (MCWS) model of Babel and Montmerle (1997), originally proposed to account for the X-ray and radio emission from Ap-Bp stars. The MCWS model postulates that disks are formed when stellar winds streaming from both magnetic hemispheres collide in the magnetic equatorial plane, producing a strong shock, an extended post shock region and a high density cooling disk. The disk is initially confined by and co-rotates with the magnetic field of the primary. Donati et al. (2001) applied this model to β Cep, a pulsating star with recurrent Be episodes. They found no basic incompatibility between the MCWS model and Be star phenomenology. In this model the disk collapses when the mass of the disk can no longer be supported by the magnetic field and predicts flow velocities back to the star in the inner regions. They propose that this collapse is the cause for the recurrent Be episodes.

As shown in Fig. 5(a), our wind solution loci limit any co-rotation region to within $r \sim 3.5R_*$. According to the MCWS model we would expect to detect motions of the disk material back to the Be star in the inner regions of the disk, but we only found evidence for an outward flow. Our analysis also indicates that such a model would require very large values of $v_r(r)$ within the co-rotating region, up to 400 km s^{-1}, i.e. much larger equatorial outflow velocities than have previously been proposed for a Be star disk. The other models predict $v_r(r)$ behavior which is consistent with previous estimates for disk outflow velocities. At present, no magnetic field has been reported for the primary of LS I +61° 303, so it is difficult to say how applicable the model is. Since LS I +61° 303 is a relatively bright ($m_V \sim 10.6$) it may be possible to set meaningful limits on the magnetic field strength of the primary from spectropolarimetry.

6. Conclusions

In this paper we have explored a new method for deriving the gas velocity and density in the Be star equatorial envelope of LS I +61°303, from the measured optically thin synchrotron radio emission at 8.3 GHz. The method yields a solution locus in the v_r, v_c plane which is a circle. Assuming five different models for $v_c(r)$, we derive the corresponding $v_r(r)$ and information about the product of $\rho(r)$ and a factor $K(r)$ that relates the 8.3 GHz flux density to the mass accretion rate by the neutron star. We also computed the $v_c(r)$ behavior expected for the $v_r(r)$ model derived by Marti and Paredes (1995) from their fit to near infrared measurements of LS I +61°303.

Although the derived densities depend on the assumed circular velocity law, the fractional change in density, $\Delta\rho_f(r)$, was found to be independent of the assumed $v_c(r)$. The variations of $\Delta\rho_f(r)$ with the ~ 4.6 year (P_2) modulation phase of LS I +61°303, indicates an outward moving density enhancement or shell in the equatorial disk with a velocity of ~ 1.0 km s^{-1}. Extrapolating back to the radius of the Be star, we conclude that ejection process begins at P_2 phase $= 0.43 \pm 0.05$. The density enhancement first becomes detectable when it reaches periastron around P_2 phase $= 0.46$. We propose that each new shell ejection may be triggered by the interaction of a short lived relativistic wind from the neutron star, with the rapidly rotating Be star. The next occurrence of this phenomena is expected around JD $\simeq 2,452,418 \pm 83$, which corresponds to the interval March 1 to August 15, 2002. The detection of a radio pulsar at this time would provide strong support for the presence of a relativistic wind. Our investigation did not find evidence for systematic negative velocities at any P_2 phase or radius, which would suggest gas returning to the star.

By comparing with independent estimates of $\rho(r)$ (Waters et al. 1988, Martí and Paredes 1995) we estimated $K(r)$. The value of $K(r)$ exhibits a decrease at both small and large values of r. The decrease at small r might reflect the relative importance of inverse-Compton losses over synchrotron losses at small radii. The decrease at large values of r may indicate a break down in the assumed power law approximation for $\rho(r)$ at a radius $> 11 \times R_*$, and suggests a much more rapid decline in disk density at larger radii.

We also estimated the mass accretion rate of the neutron star, $\dot{\mathrm{M}}_n$, from equation (1) using the derived $K(r)$ and the measured values of $S_{8.3}(r)$ averaged over all P_2 phase. Our estimates of $\dot{\mathrm{M}}_n$ are in the range $10^{-9} - 10^{-11}$ M$_\odot$ yr^{-1}. For comparison, the mass outflow rate in the Be star disk is estimated to be in the range $0.4 - 4.0 \times 10^{-7}$ (Martí and Paredes 1995). For the Mennickent circular velocity model, $\dot{\mathrm{M}}_n$ corresponds to the range ~ 0.001 to ~ 0.01 of the Eddington accretion limit for a neutron star. This translates to an expected luminosity range of $\sim 10^{35}$ to $\sim 10^{36}$ ergs s^{-1} which is comparable to estimates of the total X-ray and γ-ray luminosity for LS I +61°303.

The authors wishes to thank Jocelyn Read for assistance in the early stages of this research. The Green Bank Interferometer is a facility of the National Science Foundation operated by the National Radio Astronomy Observatory. From 1978-1996, it was operated in support of USNO and NRL geodetic and astronomy programs; after 1996 in support of NASA High Energy Astrophysics programs. The NRAO is operated by Associated Universities, Inc., under contract with the National Science Foundation. This research was supported in part by grants from the Canadian Natural Sciences and Engineering Research Council at the University of British Columbia.

REFERENCES

Babel, J. and Montmerle, T. 1997, A&A, 323, 121

Bjorkman, J.F., Cassinelli, J.P. 1992, in Nonisotropic and Variable Outflows from Stars, ASP Conference Series, ed. L. Drissen, C. Leitherer, and A. Nota, 22, 88

Bondi, H. and Hoyle, F. 1944, MNRAS, 104, 273

Donati, J.-F., Wade, G. A., Babel, J., Henrichs, H. F., de Jong, J. A., Harries, T. J., 2001, M.N.R.A.S. 326, 1265

Frail, D. A. and Hjellming, R. M. 1991, AJ, 101, 2126

Gregory, P.C., Kronberg, P.P., Seaquist, E.R., Hughes, V.A., Woodsworth, A., Viner, M.R., Retallack, D., Hjellming, R.M. and Balick, B. 1972, Nature (Phys. Sci.), 239, 114

Gregory, P. C. and Taylor, A. R. 1978, Nature, 272, 704

Gregory, P. C., Taylor, A. R., Crampton, D., Hutchings, J. B., Hjellming, R. M., Hogg, D., Hvatum, H., Gottlieb, E. W., Feldman, P.A. and Kwok, S. 1979, AJ, 84, 1030

Gregory, P. C., Xu, Huang-Jian, Backhouse, C. J., Reid, A. 1989, ApJ, 339, 1054

Gregory, P. C. 1999, ApJ, 520, 361

Gregory, P. C., Peracaula, M. and Taylor, A.R. 1999, ApJ, 520, 376

Gregory, P. C., ApJ, (in press 2002)

Howarth, I. D. 1983, MNRAS, 203, 801

Hummel, W. 2000, IAU colloquium 175, eds. M. A. Smith, H. F. Henricks, and J. Fabregat, APS Conference Series, 214, 396

Hutchings, J. B., & Crampton, D. 1981, PASP, 93, 486

Harrison, F. A., Ray, P.S., Leahy, D. A., Waltman, E. B., & Pooley, G. C. 2000, ApJ, 528, 454

Kniffen, D. A. et al. 1997, ApJ, 486, 126

Waters, L. B. F. M. 1987, ApJ, 182, 80

Leahy, D. A., Harrison, F. A., & Yoshida, A. 1997, ApJ, 475, 823

Leahy, D. A. 2001, A&A, 380, 516

Lipunov, V. M.,"Astrophysics of Neutron Stars", Springer Verlag, NY, 1992

Lipunoz, V. M. and Nazin, S. N. 1994, A&A, 289, 822

Maraschi, L. and Treves, A. 1981, MNRAS, 194, 1P

Marlborough, J.M., Zijlstra, J.W., Waters, L.B.F.M. 1997, A&A, 321, 867

Martí, J. and Paredes, J. M. 1995, A&A, 298, 151

Massi, M., Ribó, M., Paredes, J.M., Peracaula, M., & Estella, R. 2001, A&A, 376, 217

Mennickent, R. E., Vogt, N., Barrera, L. H., Covarrubias, R., Ramírez, A. 1994, A&A Suppl., 106, 427

Paredes, J. M., and Figueras, F. 1986, A&A, 154, L30

Paredes, J. M., Estalella, R., Ruis, A. 1990, A&A, 232, 377

Paredes, J.M., Martí, J., Peracaula, M. & Ribo, M. 1997, A&A, 320, L25

Peracaula, M., Gabuzda, D. C., Taylor, A. R. 1998, A&A, 330, 612

Ray, P. S., Foster, R.S., Waltman, E. B. et al. 1997, ApJ, 491, 381

Steele, I. A., Negueruela, I., Coe, M. J., Roche, P. 1998, MNRAS, 297, L5-110

Taylor, A. R. and Gregory, P. C. 1982, ApJ, 255, 210

Taylor, A. R. and Gregory, P. C. 1984, ApJ, 283, 273

Taylor, A. R., Kenny, H. T., Spencer, R. E. and Tzioumis, A. 1992, ApJ, 395, 268

Taylor, A. R., Young, G., Peracaula, M., Kenny, H. T., and Gregory, P. C. 1996, A&A, 305, 817

van den Heuvel, E. P. J. and Rappaport, S. 1987, Physics of Be stars; Proceedings of the Ninety-second IAU Colloquium, Boulder, CO, Aug. 18-22, 1986 (A88-39926 16-90). Cambridge and New York, Cambridge University Press, p. 291

van den Heuvel, E. P. J. 1994, The Evolution of X-ray Binaries, Proceedings of a conference held in College Park, MD, 1993. Edited by Steve Holt and Charles S. Day. New York: American Institute of Physics Press. AIP Conference Proceedings, Vol. 308, 1994, p.18

Waters, L. B. F. M. 1988, A&A, 162, 121

Waters, L. B. F. M., Taylor, A.R., van den Heuvel, E. P. J., Habets, G. M. H. J., Persi, P. 1988, A&A, 198, 200

Vakili, F., Mourard, D., Stee, Ph., Bonneau, D., Berio, P., Chesneau, O., Thureau, N., Morand, F., Labeyrie, A., and Tallon-Bosc, I. 1998, A&A, 335, 261

Wood, K., Bjorkman, K. S., Bjorkman, J. E. 1997, ApJ477, 926

Zamanov, R. K. 1995, MNRAS, 272, 308

Zamanov, R. K., and Martí, J. 2000, A&A, 358, L55

This preprint was prepared with the AAS LaTeX macros v5.0.

7. Appendix

In this appendix we provide a derivation of equation (12). We use as our starting point equation (11), the relevant part of which is repeated here.

$$S_{out}(r)\ v^3_{rel,out}(r) = S_{in}(r)\ v^3_{rel,in}(r) \tag{25}$$

Take the 2/3 root of each side.

$$S^{2/3}_{out}(r)\ v^2_{rel,out}(r) = S^{2/3}_{in}(r)\ v^2_{rel,in}(r) \tag{26}$$

Now substitute for $v^2_{rel,out}(r)$ from equation (9)

$$\frac{(v_n(r)^2 + v_c(r)^2 + v_r(r)^2 - 2v_n(r)v_c(r)\sin\phi(r) - 2v_n(r)v_r(r)\cos\phi(r))}{(v_n(r)^2 + v_c(r)^2 + v_r(r)^2 - 2v_n(r)v_c(r)\sin\phi'(r) - 2v_n(r)v_r(r)\cos\phi'(r))} = \frac{S^{2/3}_{out}(r)}{S^{2/3}_{in}(r)}\ , \tag{27}$$

where $\phi(r)$ is the angle between $v_n(r)$ and $v_r(r)$ on the inbound part of the orbit, and $\phi'(r)$ is the corresponding angle for the outbound portion of the orbit. Now

$$\sin\phi'(r) = \sin\phi(r) \qquad \text{and} \qquad \cos\phi'(r) = -\cos\phi(r). \tag{28}$$

After rearranging equation (27) we obtain

$$v_r(r)^2 + 2v_n(r)v_r(r)\beta(r)\cos\phi(r) + v_c(r)^2 - 2v_n(r)v_c(r)\sin\phi(r) = -v_n(r)^2, \tag{29}$$

where,

$$\beta(r) = \frac{S^{2/3}_{out}(r) + S^{2/3}_{in}(r)}{S^{2/3}_{out}(r) - S^{2/3}_{in}(r)} = \frac{(\frac{S_{out}(r)}{S_{in}(r)})^{2/3} + 1}{(\frac{S_{out}(r)}{S_{in}(r)})^{2/3} - 1}. \tag{30}$$

The equation for a circle, offset from the origin, is given by

$$(x - x_0)^2 + (y - y_0)^2 = R^2. \tag{31}$$

This can be rewritten as

$$x^2 - 2x_0x + y^2 - 2y_0y = R^2 - x_0^2 - y_0^2. \tag{32}$$

Equation (29) can thus be seen to be a circle with center at $v_r(r) = -\beta(r)v_n(r)\ \cos\phi(r)$ and $v_c(r) = v_n(r)\ \sin\phi(r)$. The radius $R(r) = \sqrt{\beta(r)^2 - 1}\ v_n(r)\ |\cos\phi(r)|$.